Engineering Structures 160 (2018) 147–160

Contents lists available at ScienceDirect

Engineering Structures

journal homepage: www.elsevier.com/locate/engstruct

Cyclic lateral load behavior of squat reinforced concrete walls

Tevfik Terzioglu[a,*], Kutay Orakcal[b], Leonardo M. Massone[c]

[a] Texas A&M Transportation Institute, Texas A&M Univ., College Station, TX 77843, United States
[b] Department of Civil Engineering, Boğaziçi University, Istanbul 34342, Turkey
[c] Department of Civil Engineering, University of Chile, Blanco Encalada 2002, Santiago, Chile

ARTICLE INFO

Keywords:
Shear
Flexure
Strength
Ductility
Squat wall
Reinforced concrete
Experiment

ABSTRACT

The level of existing research, as well as current code provisions and modeling approaches, are not adequate to characterize the behavior of squat reinforced concrete walls with shear – controlled responses. In this study, an experimental program was conducted to investigate the shear-dominated response attributes of eleven squat wall specimens; including their failure mode, lateral load capacity, ductility, hysteretic response characteristics, and deformation characteristics. Test parameters included the wall aspect ratio, the amounts of vertical and horizontal web reinforcement and longitudinal boundary reinforcement, and the level of axial load. The experimental findings are presented and discussed in this paper, with emphasis on the observed failure mode, shear strength, deformation capacity, and strength degradation characteristics of the walls tested, as well as the contribution of shear, flexural, and sliding deformations to wall lateral displacements. Comparison of the test results with backbone curves specified in performance assessment guidelines is also provided.

1. Introduction

Structural walls are widely used for improved seismic performance of reinforced concrete building structures, and are commonly designed to experience ductile flexural yielding under severe earthquakes [1]. Properly designed and detailed structural walls possess the necessary strength, stiffness, and ductility characteristics to ensure life-safety performance in a building subjected to a design-level earthquake, and to minimize damage on the structure during a service-level earthquake. An adequate design of a slender reinforced concrete structural wall requires that wall shear failure does not occur and the wall experiences a ductile flexural response under seismic excitations. However, this may not be achieved when the structural wall is relatively short, and its response is governed by shear deformations. Such walls with aspect ratios smaller than 1.5 can be used in the seismic design of low-rise buildings such as parking structures, or buildings with perimeter walls where the perimeter wall has large window openings which results in formation of squat horizontal and vertical wall segments between the openings [2].

The targeted behavior and failure mode of a well-detailed structural wall is, as aforementioned, usually flexure-controlled. However, depending on different attributes including wall geometry and aspect ratio, web and boundary reinforcement characteristics, and loading conditions, squat walls generally experience one of the three typical mode of failures: diagonal tension, diagonal compression or sliding shear [1]. Fig. 1 shows representative damage patterns for the three failure modes observed in squat walls. The diagonal tension failure mode (Fig. 1(a)) will occur whenever the transverse reinforcement amount is insufficient to carry the shear forces, or is inadequately anchored. When adequate transverse reinforcement is provided, but the wall is subjected to a high shear stress, concrete may crush under diagonal compression (Fig. 1(b)). Finally, for walls with adequate transverse reinforcement but low quantities of longitudinal reinforcement in the web, failure can be due to yielding of longitudinal reinforcement followed by growth and widening of interface cracks, leading to a sliding deformation along the base of the wall (Fig. 1(c)). This last failure mode is particularly important for walls subjected to cyclic displacement reversals.

Most of the early research on squat walls has focused on their stiffness and lateral load capacity, without characterizing other important response attributes such as shear ductility or strength degradation after capacity is reached. Some researchers [3–5] have developed empirical equations for design parameters of squat walls using test data, and others [6] have developed behavioral models that use basic principles of mechanics in order to estimate their lateral load capacity. Benjamin and Williams [7] conducted one of the pioneering experimental research studies on monotonic testing of low-rise walls with openings, for characterizing their lateral load capacity and different failure modes. Cardenas et al. [3] investigated the strength and load–deformation characteristics of walls in both high- and low-rise

* Corresponding author.
E-mail addresses: tevfikterzioglu@tamu.edu (T. Terzioglu), kutay.orakcal@boun.edu.tr (K. Orakcal), lmassone@ing.uchile.cl (L.M. Massone).

https://doi.org/10.1016/j.engstruct.2018.01.024
Received 4 October 2016; Accepted 9 January 2018
Available online 20 January 2018
0141-0296/ Published by Elsevier Ltd.

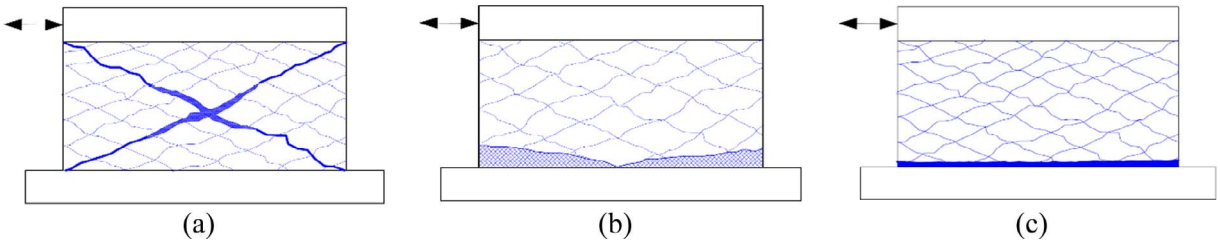

Fig. 1. Failure modes of squat walls: (a) Diagonal tension, (b) Diagonal compression, and (c) Sliding shear.

buildings. Another experimental study by Cardenas et al. [8] on low-rise walls with 1.0 aspect ratio and no boundary elements showed that the amount and distribution of web reinforcement were the major parameters affecting their lateral strength. Barda et al. [4] showed that boundary elements enhanced the post–ultimate load carrying characteristics of squat walls, and also suggested that the specimens with aspect ratios of 1/2 and less, the horizontal reinforcement did not increase the shear strength, whereas horizontal reinforcement was effective for producing a distributed cracking pattern. Based on test results, Hidalgo et al. [9] drew conclusions on the shear strength and energy dissipation capacity of squat walls.

Other research has focused on developing rational design criteria for squat walls, via investigating the effect of different parameters on their behavior and failure modes. Lefas et al. [10] investigated the cause of wall failure and suggested that shear resistance of structural walls is associated with the compression zone rather than the tensile zone of the section. Later Salonikios et al. [11] explored the applicability of ACI 318 requirements for squat walls and reported that even walls with 1.0 aspect ratio can experience flexural failure when detailed properly.

In terms of characterization of the nonlinear response characteristics of squat walls for performance assessment, in the pioneering FEMA 356 Prestandard and Commentary for the Seismic Rehabilitation of Buildings [12], particular emphasis was placed on the estimation of the shear strength of squat structural walls or wall segments in existing buildings. Orakcal et al. [13] showed that the recommendations of FEMA 356 [12] incorporate deficiencies related to consideration of the influence of axial load, the number of curtains of web reinforcement, and the amount of longitudinal boundary reinforcement on assessment of the shear strength of lightly-reinforced squat wall segments. As well, very limited information was provided in FEMA 356 [12] on the lateral load versus deformation backbone relationships for shear-controlled walls or wall segments (e.g., wall piers and spandrels), to be used in the seismic performance evaluation (e.g., pushover analysis) of existing buildings. The FEMA 356 [12] methodology to determine the envelope curve from a cyclic experimental data was shown to potentially result in underestimation of the lateral load versus displacement response characteristics for squat walls. Massone [14] showed that the backbone relationships defined in FEMA 356 [12] incorporate deficiencies related to the initial stiffness and ductility of squat wall segments, as well as their shear strength under axial load. An alternative procedure was introduced by Massone [14], which provides better estimation of stiffness and ductility of squat structural walls, as well as better representation of their lateral load–displacement response attributes. Based on the experimental research conducted by Massone [14], modified backbone curves for shear-controlled walls were first introduced as part of ASCE 41/SEI – Supplement 1 and later adopted in ASCE 41-13 [15].

Recent building codes and performance assessment guidelines (e.g. ACI 318-14 [16], ASCE 41-13 [15]) place considerable emphasis on understanding the lateral strength, stiffness, and ductility characteristics of the individual structural members, as well as their nonlinear response attributes and the modeling parameters to be used in nonlinear analysis. Most of the limited amount of existing research on analytical modeling of the nonlinear behavior of shear-controlled walls approaches the problem using one of three alternative methodologies. The first approach is the estimation of wall shear strength using the strut-and-tie modeling approach [17,18], the second is modeling of the wall response using fiber-based or multiple-spring models [2,19] that consider shear-flexure interaction, and the third is utilizing the finite element modeling approach [20,21]. While all of these modeling approaches incorporate advantages as well as limitations of their own, they are not commonly used in design or performance assessment of buildings incorporating squat walls or shear-controlled wall segments, and are not available in widely-used commercial software for nonlinear analysis. Use of the backbone curves specified in ASCE 41-13 [15], together with the shear strength calculation prescribed in ACI 318-14 [16] is therefore the more common approach used in nonlinear analysis for performance assessment.

Overall, although extensive research has been conducted on the behavior and design of slender walls, available information on the behavior of squat walls with shear-controlled responses is limited. Also, strength calculations specified in design codes and backbone curves recommended in assessment/rehabilitation guidelines may not always provide realistic estimations of shear-controlled wall response. Based on these shortcomings, this experimental study was conducted for further investigating the shear-dominated lateral load behavior and failure modes of squat walls. Test observations on important wall response characteristics are presented in this paper. Comparison of test results with backbone curves specified in performance assessment guidelines is also provided.

2. Test program

2.1. Specimen properties

Six types of squat wall specimens, comprising a total of eleven specimens (Type 1: four specimens, Type 2: three specimens, Type 3: one specimen, Type 4: one specimen, Type 5: one specimen, and Type 6: one specimen) were tested at the Bogazici University Structural Engineering Laboratory, as part of a research project initiated at the University of Chile (BU/UCH test program). Three wall aspect ratios were considered: 0.33, 0.5 and 1.0. All wall specimens had 1500 mm (59 in.) length and 120 mm (4.7 in.) thickness, with varying heights to attain different aspect ratios. The specimens were differentiated by their web reinforcement ratio, aspect ratio, the amount of boundary reinforcement, and the compressive strength of concrete. Properties of the test specimens are presented in Table 1, along with their notation. The specimens are grouped in six types (T component of the name), where each specimen type has a specific aspect ratio and specific web and boundary reinforcement amounts. For each specimen of a specific type, there is a specimen number (S component of the name). The final number in the specimen name is only related to the sequence of testing, and will be dropped in further discussion. Two of the specimens of Type 1 were tested under constant axial load, and an additional code is incorporated in their name (N component of the name): Specimen T1-N5-S1 was tested under an axial load of approximately 5% of its axial load capacity ($5\%A_g f_c'$), whereas Specimen T1-N10-S1 was subjected to an axial load of approximately $10\%A_g f_c'$.

Table 1
Properties of BU/UCH test program specimens.

Specimen	l_w (cm)	h_w (cm)	Concrete	Horizontal Reinforcement		Vertical Reinforcement		Boundary Reinf.		$f_{y,web}$	$f_{y,bound.}$
			f'_c (MPa)	Bars	ρ_t (%)	Bars	ρ_l (%)	Bars	ρ_b (%)	(MPa)	(MPa)
T2-S1-1	150	75	19.3	ϕ8@125	0.68	ϕ8@125	0.68	4ϕ16	5.15	481	440
T2-S2-3	150	75	25.8	ϕ8@125	0.68	ϕ8@125	0.68	4ϕ16	5.15	481	440
T2-S3-4	150	75	29	ϕ8@125	0.68	ϕ8@125	0.68	4ϕ16	5.15	584	473
T3-S1-5	150	75	32.1	ϕ8@125	0.68	ϕ8@125	0.68	2ϕ8	0.65	584	584
T4-S1-6	150	50	34.8	ϕ8@125	0.68	ϕ8@125	0.68	4ϕ14	3.95	584	519
T5-S1-7	150	150	35	ϕ8@125	0.68	ϕ8@250	0.34	4ϕ22	9.75	584	528
T6-S1-8	150	150	22.6	ϕ8@125	0.68	ϕ8@125	0.68	4ϕ22	9.75	584	528
T1-S2-9	150	75	24	ϕ8@250	0.34	ϕ8@250	0.34	4ϕ16	5.15	584	473
T1-N5-S1-10	150	75	26.3	ϕ8@250	0.34	ϕ8@250	0.34	4ϕ16	5.15	584	473
T1-N10-S1-11	150	75	27	ϕ8@250	0.34	ϕ8@250	0.34	4ϕ16	5.15	584	473
T1-S1-2	150	75	23.7	ϕ8@250	0.34	ϕ8@250	0.34	4ϕ16	5.15	481	440

Note: 1 MPa = 0.145 ksi.
1 cm = 0.394 in.
ϕ8 (8 mm diameter) = bar size between U.S. No. 2 & No. 3; ϕ16 (16 mm diameter) = U.S. No. 5.

Although of the same Type, Specimens T2-S1 and T2-S2 differed in terms of anchorage conditions of horizontal web reinforcement: Specimen T2-S1 had U-cap hooks at the ends of the horizontal web bars, while specimen T2-S2, as well as all other specimens, had 180° hooks at the end of the horizontal bars Another variation exists in specimen T1-S2, in which the longitudinal boundary reinforcement was confined with ties, whereas no confinement was provided for other specimens. During construction of the specimens, there were some concerns on the placement of the concrete during casting of specimen T2-S2. Therefore, an identical specimen named as T2-S3 was constructed, Fig. 2 shows the reinforcement detail for the Type 1 and Type 2 specimens, as an illustrative example. A more detailed description of the test specimens and the experimental program can be found elsewhere (Terzioglu [22]).

2.2. Test setup

The specimens were tested in an upright position, as shown in Fig. 3. The specimen pedestals were fixed to a strong floor at the base and the lateral load was applied on a reinforced concrete loading beam at the top. An out-of-plane support frame was provided to prevent twisting of the specimens during lateral loading. The axial load was applied using prestressed steel cables anchored in the bottom pedestal of the specimens. Reversed cyclic lateral loading was applied at the top of each specimen, resulting in a single-curvature loading condition. Lateral loading was displacement-controlled (except for the very initial loading cycles), and three full cycles were applied at each target drift level. First two or the three initial target drift (or lateral load) levels differed from one specimen to next. Following the initial drift levels to small displacements, the specimens were subjected to target drift levels of 0.05%, 0.1%, 0.15%, 0.2%, 0.3%, 0.4%, 0.6%, 0.8%, 1.0%, 1.2%, 1.4%, 1.6%, 1.8%, 2.0%, 2.4%, and 3.2%. Depending on their residual lateral load capacity, one or two additional drift levels were imposed on some of the specimens.

2.3. Instrumentation

The instrumentation used during this test program allowed measuring loads, displacements, average deformations, and strains at various locations on the wall specimens. LVDTs were mounted horizontally between each specimen and an external reference frame affixed to the bottom pedestal of the specimen, so that no correction on the measured lateral top displacement was required to account for pedestal sliding or rotation. LVDTs were also installed on the specimens diagonally (in an "X" configuration) for shear deformation measurements, as well as vertically for measuring flexural deformations and rotations along the height of the specimens. Additional displacement sensors were mounted horizontally between each wall specimen and the bottom pedestal for measuring sliding shear deformations at the wall-pedestal interface. Fig. 4(a) shows representative sensor layout for a specimen with an aspect ratio of 0.5. A similar instrumentation scheme was used for all tests. As well, strain gauges were installed on the reinforcing bars of the wall specimens at various locations. The strain gauge measurements were primarily used for monitoring yielding in a specific rebar. A total of thirteen strain gauges were installed on each specimen, as shown in Fig. 4(b).

2.4. Experimental observations and failure modes

During the tests, a correlation was observed between the failure type of each specimen and yielding of wall transverse (horizontal) reinforcement. The specimens that had low transverse web reinforcement ratio (Type 1) failed in diagonal tension, and the transverse reinforcement of these specimens yielded during the tests. On the other hand, the specimens that had high web reinforcement ratio (Types 2, 4, and 6) failed in diagonal compression, and none of the transverse reinforcing bars yielded during testing. The specimen with low amount of boundary reinforcement (Type 3) experienced sliding shear failure at the wall-pedestal interface, and also did not show any yielding of transverse reinforcement, as expected.

2.4.1. Diagonal tension failure

Type 1 specimens had 0.34% vertical and horizontal web reinforcement ratios with 4-ϕ16 longitudinal bars at each boundary. In all Type 1 specimens, the first major diagonal tension crack formed from corner to corner, during the first cycles of the 0.1% drift level, although initial cracking was observed earlier.

Specimen T1-S1 (Fig. 5(a)) presented crushing of the concrete at the bottom corners at 0.8% drift level. Both longitudinal (vertical) and transverse (horizontal) reinforcing bars yielded after reaching the ultimate load capacity at 1% drift level. Crushing and spalling of the concrete concentrated at the wall center, and strength degradation initiated at 1.2% drift. The main diagonal cracks opened and closed during every cycle, and eventually crushing of concrete propagated along the diagonal tension and compression struts, indicating a general diagonal tension type of squat wall failure.

Specimen T1-S2 had a similar configuration to T1-S1. However, confinement was provided in the boundary regions, with ties at 75 mm spacing along the height of the wall. For this specimen, crushing of the concrete initiated at the center of a diagonal strut. It was expected that the orthogonal diagonal strut would also experience crushing when the load was reversed. However, during following cycles, concrete crushed at the bottom of the wall, indicating diagonal compression failure,

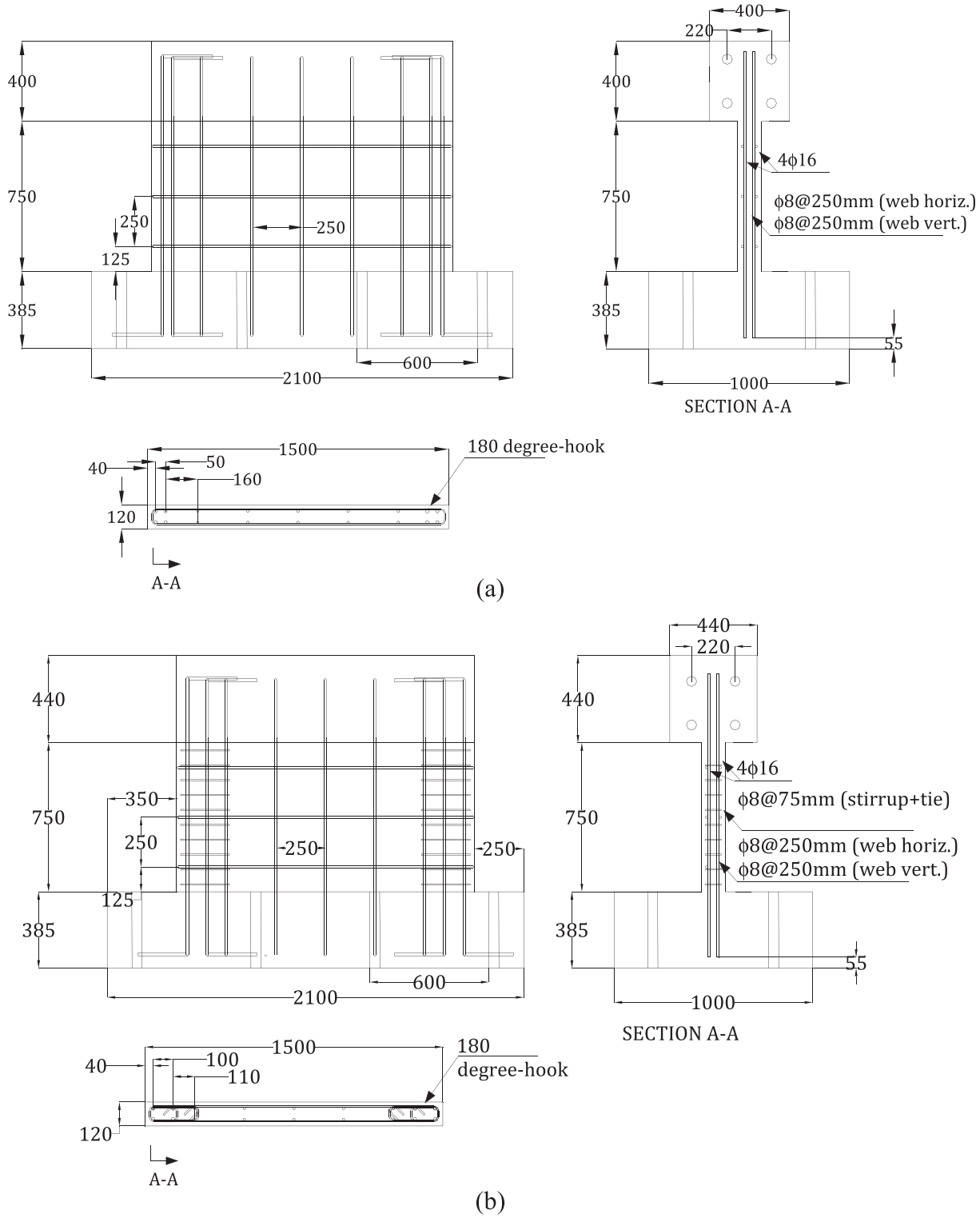

Fig. 2. Wall geometry and reinforcement: (a) Type 1 specimen and (b) Type 2 specimen. Note: All units are in mm. 1 mm = 0.0394 in.

which prevented crushing along the second diagonal strut at the wall center. The specimen reached ultimate strength and failed in diagonal tension, but at larger drifts, concrete crushing at the bottom corner propagated along the wall base, resembling diagonal compression failure (Fig. 5(b)).

Specimen T1-N5-S1 was subjected to an axial load of $5\%A_g f_c'$ (240 kN [54kips]). For this specimen, a cracking pattern and crushing mechanism similar to specimen T1-S1 was observed. Crushing of the concrete was initiated at the center of the specimen, indicating that the mode of failure was diagonal tension. At large drift levels, the bottom corners of the specimen crushed due to the compressive stresses on the diagonal struts.

The second specimen with axial load, T1-N10-S1, was tested under an axial load of $10\%A_g f_c'$ (480 kN [108kips]). Higher drift levels than 1.4% could not be applied on this specimen due to sudden degradation of the lateral load just after the ultimate lateral load capacity was reached. The propagation and distribution of the cracks were similar to specimen T1-N5-S1, excluding an additional crack that formed at 0.8%

Fig. 3. Test setup.

drift. At that drift level, a horizontal crack formed connecting two diagonal cracks; one coming from the bottom corner and the other from the opposite top corner, followed by crushing of concrete around these diagonal and horizontal cracks. Evidently, the large level of axial load changed the orientation of the main diagonal crack, making it horizontal at the region close to the wall center. After reaching the peak capacity, the specimen experienced very sudden degradation in lateral load capacity, together with crushing and sliding along then main three-segment crack, with no crushing observed elsewhere (Fig. 5(c)).

2.4.2. Diagonal compression failure

Type 2 specimens had vertical and horizontal web reinforcement ratios of 0.68% and 4-ϕ16 longitudinal bars at each boundary. Specimen T2-S1 had U-caps, while T2-S2 having 180-degree hooks at the ends of the horizontal reinforcing bars to provide adequate anchorage. The difference in the anchorage detail did not significantly influence the observed behavior. An additional specimen with identical to specimen T2-S1, which was named as T2-S3, was tested, to confirm its behavior. Similar experimental results were obtained for the two identical specimens.

For Specimens T2-S1 and T2-S3, the main diagonal cracks first formed at 0.1% drift level in both positive and negative loading directions. At higher drift levels, crack formation progressed in the previously uncracked regions of the specimens, and the main diagonal cracks extended from bottom pedestal to top beam. Unlike diagonal tension failure, where crushing occurs along the diagonal struts, the concrete started to crush at the bottom corners of the walls when the lateral load capacity was reached at approximately 1–1.2% drift. As Park and Paulay [23] first discussed, it is almost impossible to have diagonal tension failure mode when a squat wall has a high ratio of transverse (horizontal) reinforcement. Although the diagonal tension cracks had formed, they did not substantially widen, and the specimens experienced a diagonal compression failure mode under combined shear and flexural effects, since the large amount of transverse reinforcement prevented the widening of the main diagonal cracks and crushing along diagonal compression struts between the cracks. Crushing was first observed at the bottom corners of the wall, where the first inclined cracks were formed. After crushing of the corner regions, the effective shear area that resists shear sliding was reduced. The crushing of the concrete then propagated inwards, along the wall-pedestal interface, while the lateral load was maintained at an almost constant residual strength of approximately 10% of the peak capacity. Eventually, the entire base of the wall crushed, and crushing extended upwards towards the center of the wall (Fig. 5(d)).

Specimen T2-S2 was loaded to larger drift levels (7%) compared to others of the same Type. After the concrete crushing, which initiated at the bottom corners and propagated towards the wall center at the base, the wall underwent sliding along the crushed base, maintaining its residual lateral strength. This observation indicates that the residual strength of the wall was not associated with concrete stresses, but by the dowel and kinking effects on the vertical reinforcement.

Other three types of specimens (Types 4, 5, and 6), for which the common parameter was the horizontal web reinforcement ratio (0.68%), also experienced diagonal compression failure. Specimen T4-S1 had an aspect ratio of 1/3, which differentiated it from the rest. The crack formation and alignment on this specimen was similar to the Type 2 specimens. Strain gauge data showed that the horizontal web reinforcement yielded at 0.6% drift level, when it reached peak lateral load capacity. The boundary reinforcement then yielded at 0.8% drift. Afterwards, concrete crushing propagated along the wall length at the base, indicating diagonal compression failure.

Type 5 and 6 specimens were comparatively slender specimens, with an aspect ratio of 1.0. Initial diagonal cracks on these specimens developed at 0.4% drift level and extended in a more horizontal manner at the base of the wall, resembling flexural cracks at the wall-pedestal interface. The diagonal tension cracks were prevented from widening by the significant amount of horizontal web reinforcement (0.68%). While diagonal compression stresses initiated crushing of concrete at the center of the wall base, the bottom corners of the specimen also crushed under flexural compressive stresses. Evidently, the specimen failed under a combined shear and flexure mode. Fig. 5(e) shows the crushing of concrete in Specimen T5-S1. Specimen T6-S1 showed similar behavior, but with a larger lateral load capacity (15% larger capacity than T5-S1) and a better distributed cracking pattern (more frequent cracks), which may be attributed to the larger vertical web reinforcement ratio of 0.68%.

2.4.3. Sliding shear failure

Specimen T3-S1 was designed to have the same web reinforcement ratio as the Type 2 specimens, but it had only 2–ϕ8 vertical bars at the boundaries, which was intentionally kept low to observe either a flexural yielding or a sliding shear failure mode at the base of the wall.

At a drift level of 0.1%, a few initial inclined cracks formed on the specimen. This was followed by formation of a horizontal crack at the wall-pedestal interface, which initiated at the wall boundaries. The lateral load capacity was reached at 0.6% drift, when the lateral load was approximately 380 kN (85 kips). At this drift level, the horizontal crack at the wall-pedestal interface had extended along the entire length of the wall base. At larger drifts, the interface crack progressively widened, and the wall started experiencing sliding shear failure along the interface crack, where the concrete also started crushing (Fig. 5(f)). The strain gauge data showed that none of the horizontal web reinforcement yielded during the test, whereas all boundary reinforcement yielded at 0.4% drift, and all vertical web reinforcement yielded at 0.6% drift. Flexural cracking and yielding of longitudinal reinforcement at the wall-pedestal interface triggered the sliding shear failure mechanism at the base of the wall. At 1% drift, the interface crack had widened significantly and the concrete started crushing along the interface. During successive loading cycles after 1.2% drift, the vertical reinforcing bars fractured one by one. At the end of the test, all of the vertical rebars had fractured at the interface. The strength degradation of the wall after the peak capacity was gradual, possibly due to kinking

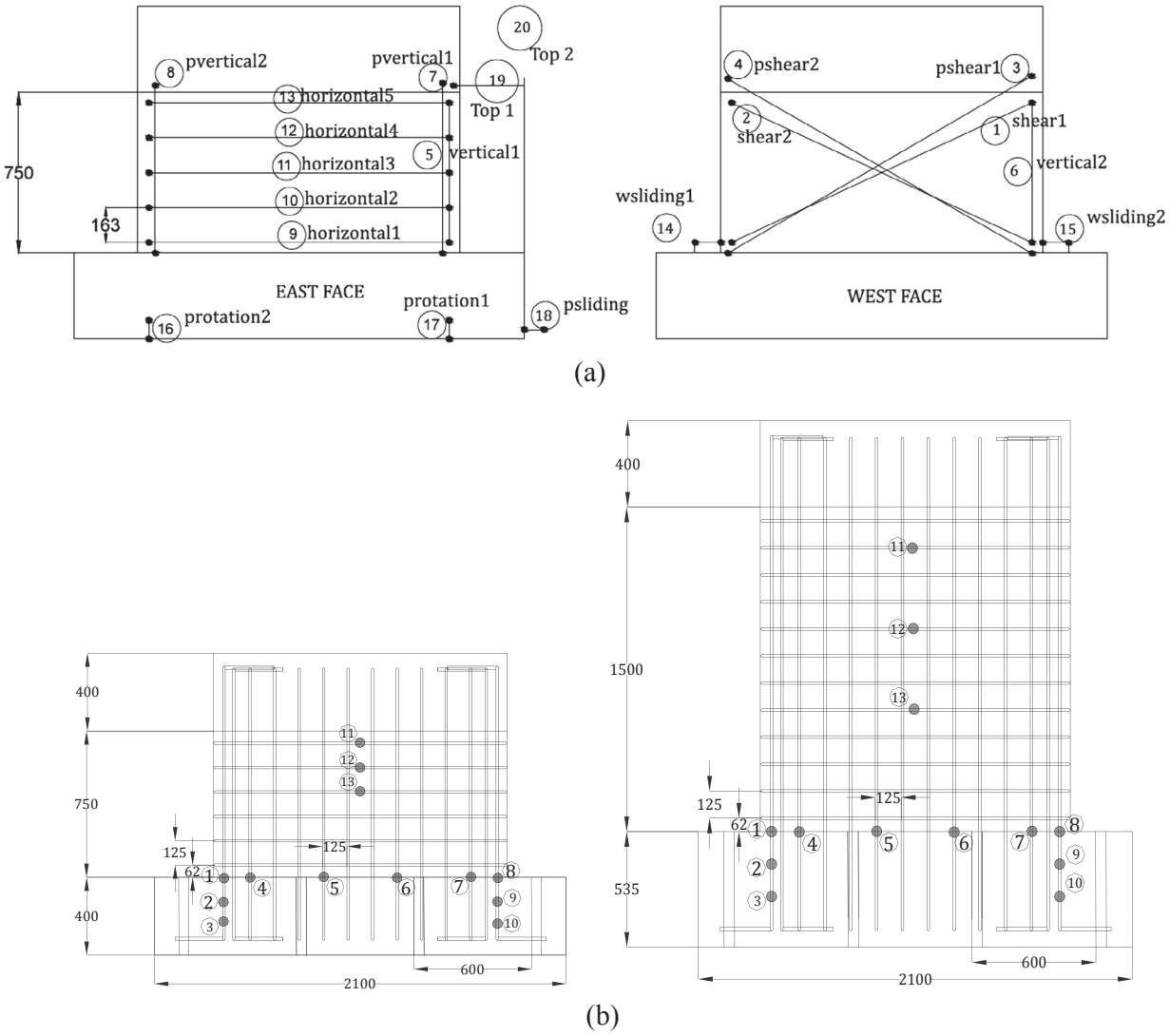

Fig. 4. Instrumentation layout: (a) LVDT layout for 0.5 aspect ratio specimens, (b) Strain gauge locations. Note: All units are in mm. 1 mm = 0.0394 in.

of the vertical rebars during sliding of the specimen. In this test, as depicted in a further section, the main deformation component was sliding along the wall-pedestal interface, which exhausted the deformation capacity of the vertical reinforcing bars, leading to their fracture.

2.5. Shear, flexural, and sliding shear deformation components

The flexural and shear deformation contributions to the top lateral displacement of the wall specimens were calculated using the measurements obtained for average rotations and shear distortions, respectively. The displacement transducers mounted on each wall segment for measuring shear and flexural deformations (i.e., local sensors) were removed at large drift levels to avoid damaging the sensors. Additional transducers were mounted between the bottom pedestal and top loading beam of each specimen (i.e., global sensors) to measure shear and flexural deformation contributions to overall top displacement over the entire range of drift levels, since these sensors could be left in place during the entire duration of each test (Fig. 4).

The flexural top displacement of each specimen was calculated by double-integrating over the wall height, the curvature distribution measured along the height of the specimen. The average curvatures along wall height were measured using the pairs of vertical sensors mounted at the wall boundaries (Fig. 4). For the flexural deformation measurements, the center of rotation of a specific wall section (or entire wall segment) was assumed to be at 0.33h from the bottom, where h is the height of the wall section, since this approach represents the center of rotation of a cantilever wall that shows linear elastic flexural behavior. The flexural deformations were calculated using the series of vertical sensors attached to the wall segment (local sensors), as well as the sensors mounted between the bottom pedestal and top beam (global sensors).

The shear deformation component of the wall lateral displacement was determined using a pair of sensors (LVDTs) mounted diagonally on each specimen. The shear displacement was calculated using measurements from the diagonal sensors only, without the correction proposed by Massone and Wallace [24] for removing the flexural deformation contribution from the shear distortion measurement, since this correction was not expected to have a significant impact on the measurements for the squat wall specimens with shear-controlled responses. Data from the diagonal sensors mounted on the wall segment (local sensors), as well as the ones attached to the bottom pedestal and top beam (global sensors) were used. The sliding shear component of wall lateral displacement was also measured using the horizontal sensors mounted at the wall-pedestal interface. The sliding shear deformation at the interface can also be calculated by subtracting shear deformation measured by the local diagonal sensors from that measured by the global diagonal sensors.

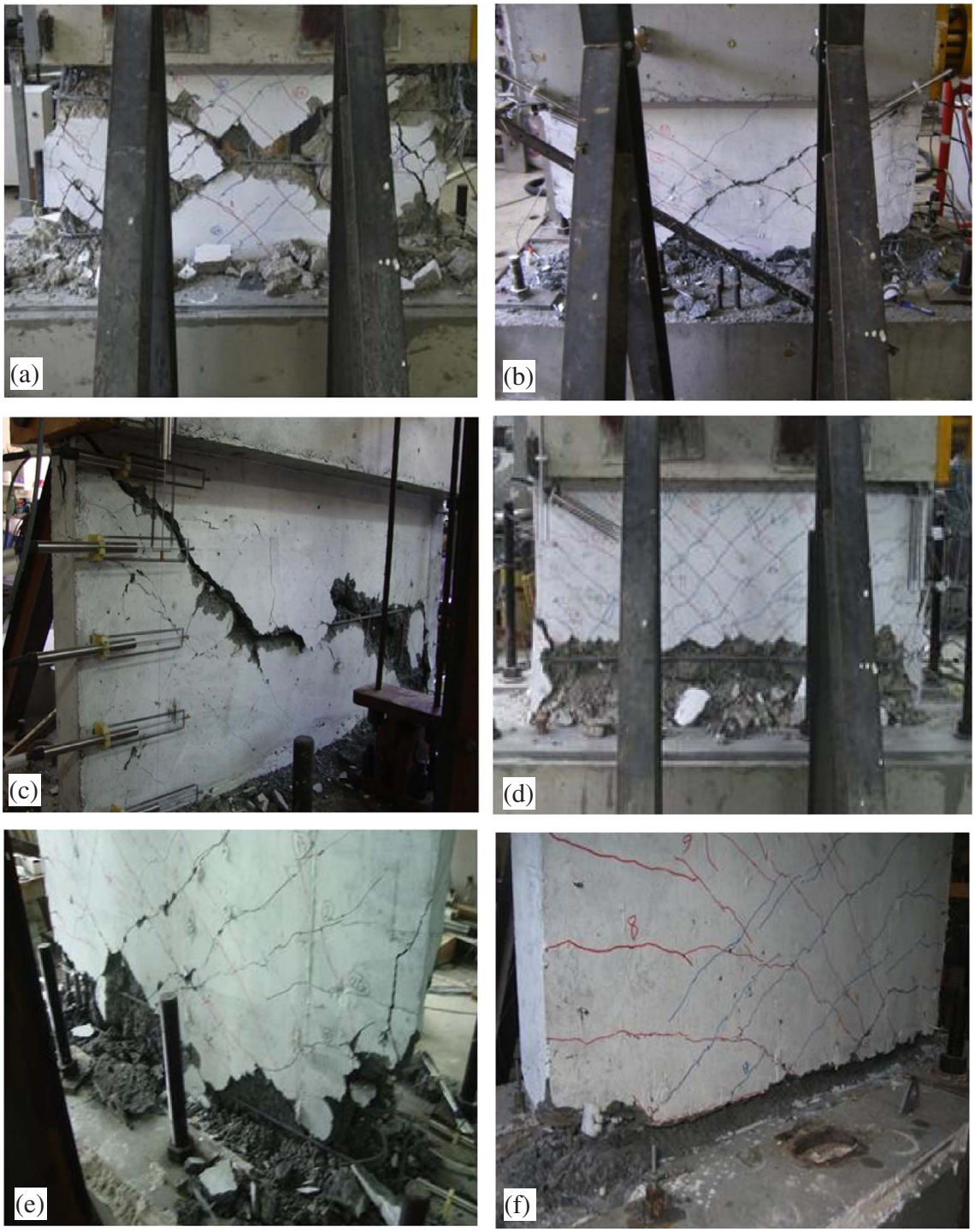

Fig. 5. Failure Modes: Diagonal tension – (a) T1-S1, (b) T1-S2, (c) T1-N10-S1; Diagonal compression – (d) T2-S1, (e) T5-S1; Sliding shear – (f) T3-S1.

2.5.1. Diagonal tension specimens

Fig. 8(a–c) compares the flexural, shear, and sliding deformation components to the top lateral displacement of specimen T1-S1. Only the flexural deformation component was measured using the sensors mounted on the pedestal and beam (global sensors), which accounts for the flexural deformation along wall height, as well as the rotation at the wall-pedestal interface. Most of the top lateral displacement is due to shear deformations. The flexural deformation component of the response remains practically linear elastic. The shape of the hysteresis loops and the pinching properties of the shear deformation component of the response resembles the overall lateral load – displacement response, indicating that the behavior of the wall was dominated by shear (diagonal tension) deformation. The sliding shear deformation component of the response is close to that of flexural deformation.

The other specimens that experienced the same failure mode (i.e., Type 1 diagonal tension specimens) presented similar behavior, with shear deformation being the main component of lateral displacement. For example, the deformation contributions to wall lateral displacement are compared in Fig. 9 (a) for specimen T1-N5-S1. In this case, the contributions are shown only at peak drift levels in positive and negative loading directions, for the deformation components (shear, flexure, sliding and wall-pedestal-interface rotation) measured using the local

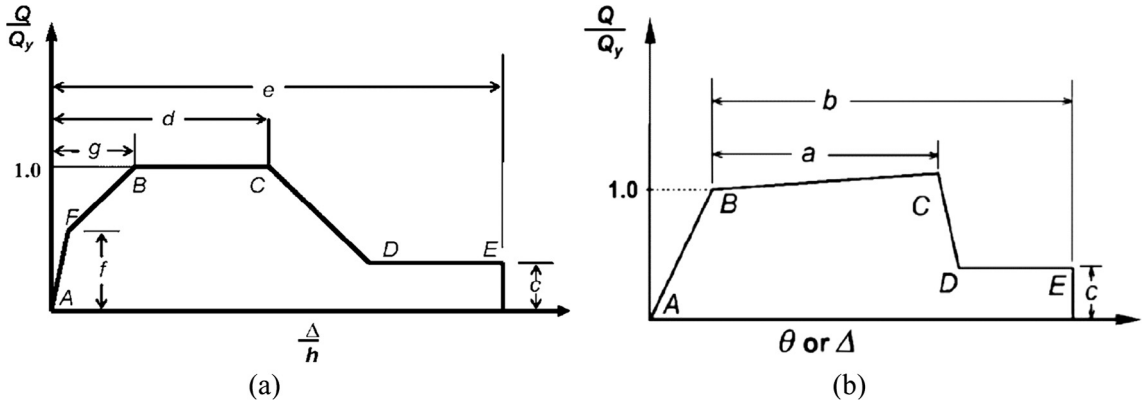

Fig. 6. Generalized force-deformation relations in ASCE41-13 [15]: (a) Backbone relation for shear-controlled RC walls, (b) Backbone relation for flexure-controlled RC walls.

sensors attached on the wall segment, until reliable data was collected. At small drift levels, the shear deformation component has the largest contribution on the response, although the wall-pedestal-interface rotation also presents a significant contribution. Figs. 9 and 10 present the contribution of different deformation components measured using the local and global sensors, respectively, for selected specimens. In Fig. 9, perfect correlation of the total of the local deformation measurements with the externally-measured lateral top displacement of the wall is indicated by a diagonal dashed line. The good agreement in Fig. 9 between the sum of the local deformation measurements with the measured lateral top displacement validates the local deformation measurement method used. Slightly larger lateral displacement obtained using the sum of the local deformation measurements can be explained in part by the fact that the correction suggested by Massone and Wallace [24] on the shear deformation measurement, which reduces the shear deformation when the center of flexural rotation does not occur at wall center, was not applied.

2.5.2. Diagonal compression specimens

Fig. 9(b) shows the local flexural, shear, sliding, and wall-pedestal-interface rotation deformation contributions to top lateral displacements at peak drift levels in the positive and negative loading directions for specimen T2-S2, which failed in diagonal compression. Similarly to the Type 1 specimen failing in diagonal tension, at small drift levels, the shear deformation contributes mostly to the response, with another significant contribution from the wall-pedestal-interface rotation. At large drift levels (Fig. 10(a)), measurements from the global sensors show that the shear deformation component dominates the top displacement of the wall.

Similarly, for the other specimens that experienced diagonal compression failure, the main contribution to top displacement comes from shear deformation. The specimens with higher aspect ratio (Types 5 and 6) show a higher contribution of flexural deformation (measured by local sensors) at relatively low drift levels (Fig. 9(c)). However, when the shear and flexural deformation components measured by the global sensors at large drift levels are observed (Fig. 10(b and c)), once degradation of capacity is triggered (at around 15–20 mm [0.6–0.8 in.] top displacement), the almost identical contributions of global shear (shear and sliding) and global flexural (flexural and wall-pedestal-interface rotation) deformations converts into consolidation of the shear deformation component. The larger flexural deformation contribution observed for Specimen T5-S1 (Fig. 10(b)) can be correlated to the more ductile response of such specimen, compared to specimen T6-S1 (Fig. 10(c)), which had a higher vertical web reinforcement ratio.

2.5.3. Sliding shear specimen

Specimen T3-S1 had only 2-ϕ8 vertical bars at the boundaries, and failed due to sliding shear at the wall base. Fig. 8(d–f) compares the flexural (global), shear (global), and sliding (local) deformation components of the lateral load vs. top displacement response. In this case, the flexural deformation component (wall flexure and wall-pedestal-interface rotation) of the response is more significant, with the flexural deformation reaching approximately 50% of the shear deformation. The shear deformation component shown in the figure corresponds to measurements recorded by the global sensors, since the local sensors presented very small shear (diagonal tension) deformation. The similar magnitude observed between the global shear and local sliding shear deformation components validates the small shear deformation measured by the local sensors, and confirms that the total shear deformation of the wall is governed by sliding shear at the base. The observed failure mode of this specimen was sliding shear; however, the specimen apparently also experienced significant amount of flexural deformation. The sliding shear deformation response shows systematic hysteresis loops that resembles the shape of the overall lateral load vs. top displacement response of the wall.

Fig. 9(d) compares the deformation contributions to wall lateral displacement for Specimen T3-S1 at peak drift levels in positive and negative loading directions, for the deformation components (shear, sliding, and flexure + wall-pedestal-interface rotation) measured using the local sensors attached on the wall. The figure indicates that the main contribution to lateral displacement comes from the flexural deformation (and interface rotation) at small drift levels. However, the sliding shear deformation component starts building up a larger contribution at around 5 mm (0.2 in.) of top displacement (0.6% drift), which corresponds to the initiation of significant degradation of the lateral load, and therefore failure due to sliding shear. Sliding shear deformation contributes by approximately 40% of the top displacement of the wall, at 1% drift. The asymmetry observed in the overall load vs. displacement response of the specimen in positive and negative loading directions (Fig. 7(f)) is also noticeable in the flexural deformation contributions presented in Fig. 9(d) which shows that flexural deformation of the wall was larger in one direction.

Fig. 10(d) presents the global shear (including sliding) and flexural (including wall-pedestal-interface rotation) deformation contributions to lateral displacement of Specimen T3-S1, over all drift levels. For this specimen, although the flexural deformation component is larger compared to other tests, due initial flexural yielding at small drift, as degradation in lateral load progresses during large drifts, the lateral displacement localizes in the global shear deformation component, due to sliding shear at the base of the wall.

2.6. Assessment of lateral load–displacement response

For evaluation of the load–displacement response characteristics of the wall specimens, the nominal shear strength of each specimen was first calculated using the shear strength provisions provided in ACI 318-14 [16] Section 18.10.4. Geometric and material properties and reinforcement ratios used for nominal shear strength calculations are

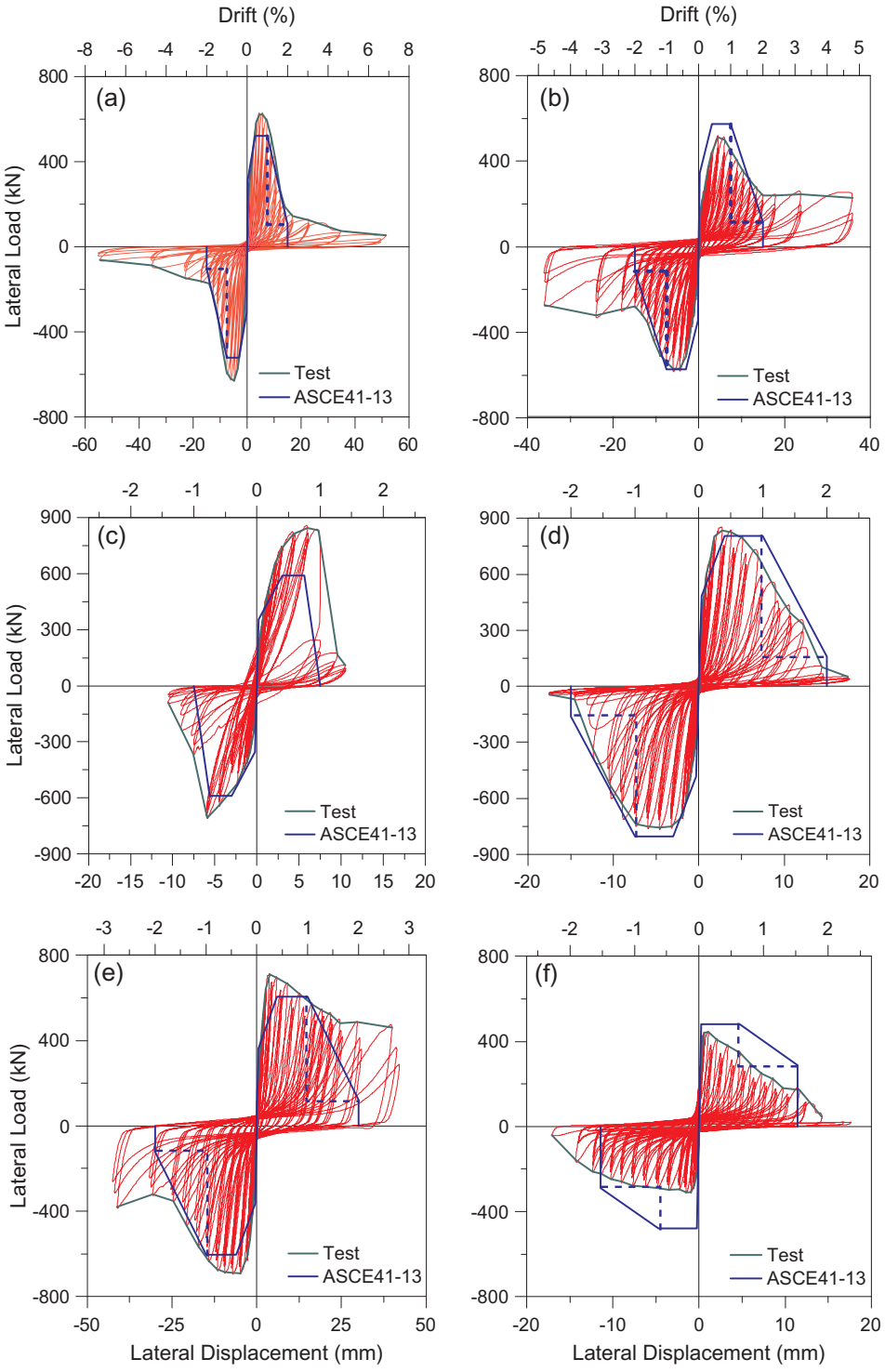

Fig. 7. Load vs. Displacement: Diagonal tension – (a) T1-S1, (b) T1-S2, (c) T1-N10-S1; Diagonal compression – (d) T2-S3, (e) T5-S1; Sliding shear – (f) T3-S1.

listed in Table 1. Comparison of the test results with the nominal shear strength calculations ($V_u/V_{n,\ ACI\text{-}318}$), as well as the cracking shear capacities, drift capacities, and ductility characteristics of the specimens are presented in Table 2. Per ASCE 41-13, the nominal shear strength of a squat wall calculated using ACI-318 Section 18.10.4 should be based on the minimum value of $\rho_t f_{yt}$ and $\rho_l f_{yl}$. Therefore, for the nominal shear strength calculation of Specimen T5-S1 the minimum of transverse and longitudinal reinforcement ratios (0.34%), was used. Overall, the ACI 318-14 nominal shear strength predictions are appropriate for the wall specimens tested (excluding the sliding shear Specimen T3-S1), but they tend to be conservative for the specimens tested under axial load (T1-N5-S1 and T1-N10-S1). On average, the specimens that failed in diagonal compression experienced an average shear stress of approximately $0.82\sqrt{f'_c}$ (MPa) ($9.9\sqrt{f'_c}$ (ksi)) at the experimentally-measured lateral load capacity, whereas the maximum average shear stress was approximately $0.68\sqrt{f'_c}$ (MPa) ($8.2\sqrt{f'_c}$ (ksi)) on the diagonal tension specimens with no axial load, $0.85\sqrt{f'_c}$ (MPa) ($10.2\sqrt{f'_c}$ (ksi)) on the diagonal tension specimens with axial load, and $0.38\sqrt{f'_c}$ (MPa) ($4.6\sqrt{f'_c}$ (ksi)) on the sliding shear specimen. Considering the shear stress level on the diagonal compression specimens, the ACI 318-14 upper limit on wall average shear stress of $0.83\sqrt{f'_c}$ (MPa) ($10\sqrt{f'_c}$ (ksi)) is appropriate. Nevertheless, it is interesting to observe that the

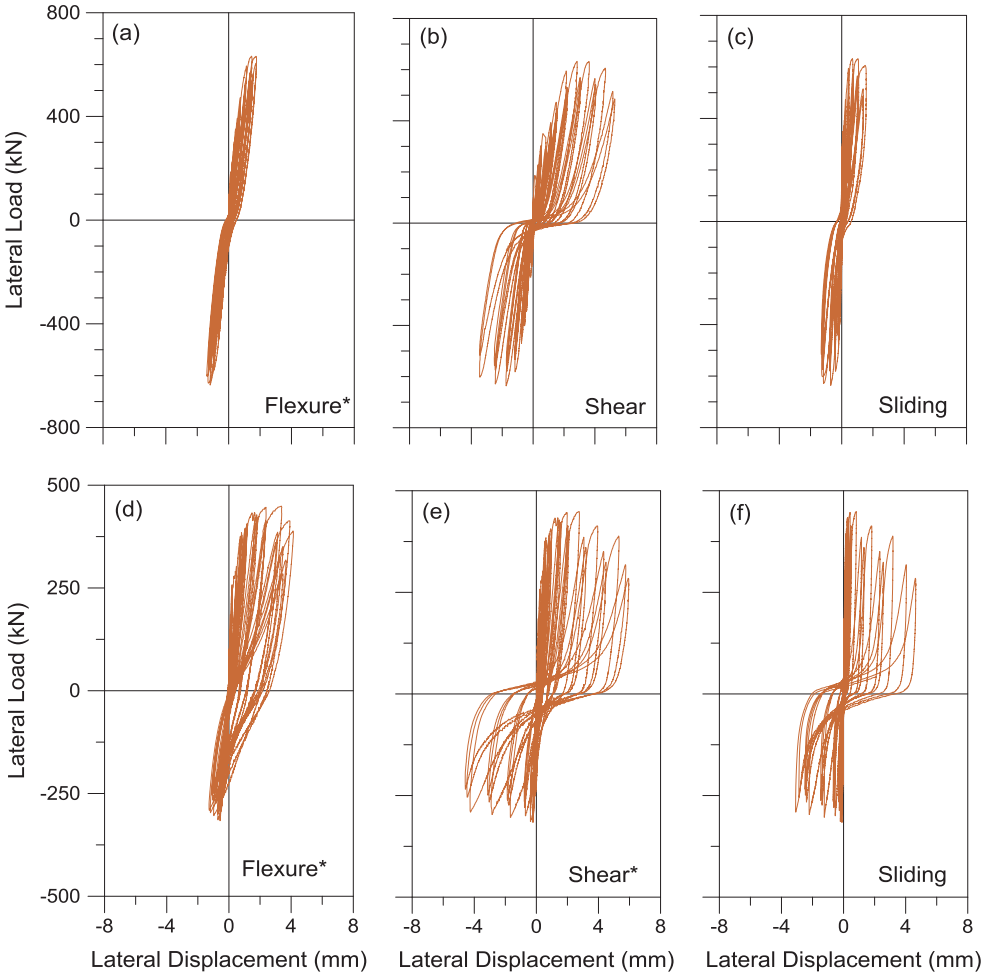

Fig. 8. Load vs. deformation responses: T1-S1 – (a) Flexure (global), (b) Shear (local), (c) Sliding (local); T3-S1 – (d) Flexure (global), (e) Shear (global), (f) Sliding (local).

specimens with axial load, although subjected to high shear stress level during testing, failed in diagonal tension due to their relatively low transverse reinforcement ratio.

Nominal shear friction capacities ($V_{n,ACI-SF}$) of the specimens were also calculated per ACI 318-14 [16] Section 22.9.4, the purpose of which is to provide design methods where it is appropriate to consider shear transfer across a given plane, such as an existing crack or potential crack or an interface between dissimilar materials and components. The coefficient of friction, μ was taken as 1.4λ (where $\lambda = 1$), as specified for monolithically-cast normal weight concrete. The calculated shear friction capacities of each specimen are listed in Table 2. Only Specimen T3-S1, which experienced sliding shear failure, has a lower shear friction capacity compared to its nominal shear strength.

The nominal moment capacities of the wall specimens were also calculated per ACI 318-14 [16] Section 22.2 to compare their nominal flexural and shear lateral load capacities. Actual (measured) material properties provided in Table 1 were used in the calculations. Nominal flexural lateral load capacities were calculated considering the single curvature (cantilever) loading condition imposed during the tests as, $V_{n,ACI-FLEX} = M_n/(wall\ height + beam\ height/2)$. Table 2 includes the nominal flexural lateral load capacities of the walls. The results show that all specimens have higher flexural lateral load capacities compared to their ACI 318 nominal shear strengths, and shear-friction capacities, with the exception of Specimen T3-S1, which suffered sliding shear failure. Yet, this specimen reached neither its nominal flexural capacity nor its shear-friction capacity, and experienced premature sliding shear mode of failure triggered by flexural yielding at the base of the wall.

The overall lateral load vs. top displacement responses of representative specimens were compared with the linearized backbone curves recommended in ASCE 41-13 [15]. The multi-linear backbone curve shown in Fig. 6(a) is suggested by ASCE 41-13 to model shear-controlled wall behavior. The curve incorporates an initial effective stiffness of $0.4E_cA_w$ (A-F), as suggested in ASCE41-13 Table 10-5, up to 60% of the expected nominal shear strength (calculated per ACI 318-14 Section 18.10.4), followed by a reduced (post-cracked) stiffness (F-B), reaching the nominal shear strength at a total drift ratio 0.4%. For walls with axial loads below $5\%A_gf'_c$, strength degradation (parameter d) starts at 1% drift, with a sudden reduction in lateral load to point D (C–D), and a residual strength of 20% of the expected nominal shear strength is specified up to a drift level of 2% (E). On the other hand, ASCE 41-13 Commentary 10.3.1.2.2 recommends a linear strength degradation behavior from point C to E, for modeling of the post-peak lateral load response. Both approaches are acceptable for generating backbone relationships for concrete components. For walls with axial loads equal or greater than $5\%A_gf'_c$, strength degradation starts at 0.75% drift level with a linear reduction in the lateral load to zero at 1% drift level.

The lateral load behavior and failure modes of all of the wall specimens were governed by shear, and all specimens exhibited brittle behavior, except specimen T3-S1. Since this specimen failed in sliding shear and had a flexural lateral load capacity smaller than its shear strength or shear-friction capacity, the ASCE 41-13 backbone relationship for this specimen was generated as flexure-controlled, as shown in Fig. 6(b), using the modeling parameters provided in ASCE 41-13 Table 10-19.

Fig. 7 compares the envelop curves of the experimental load-displacement responses with the ASCE 41-13 backbone curves for several representative specimens. In the plots, the solid line represents the

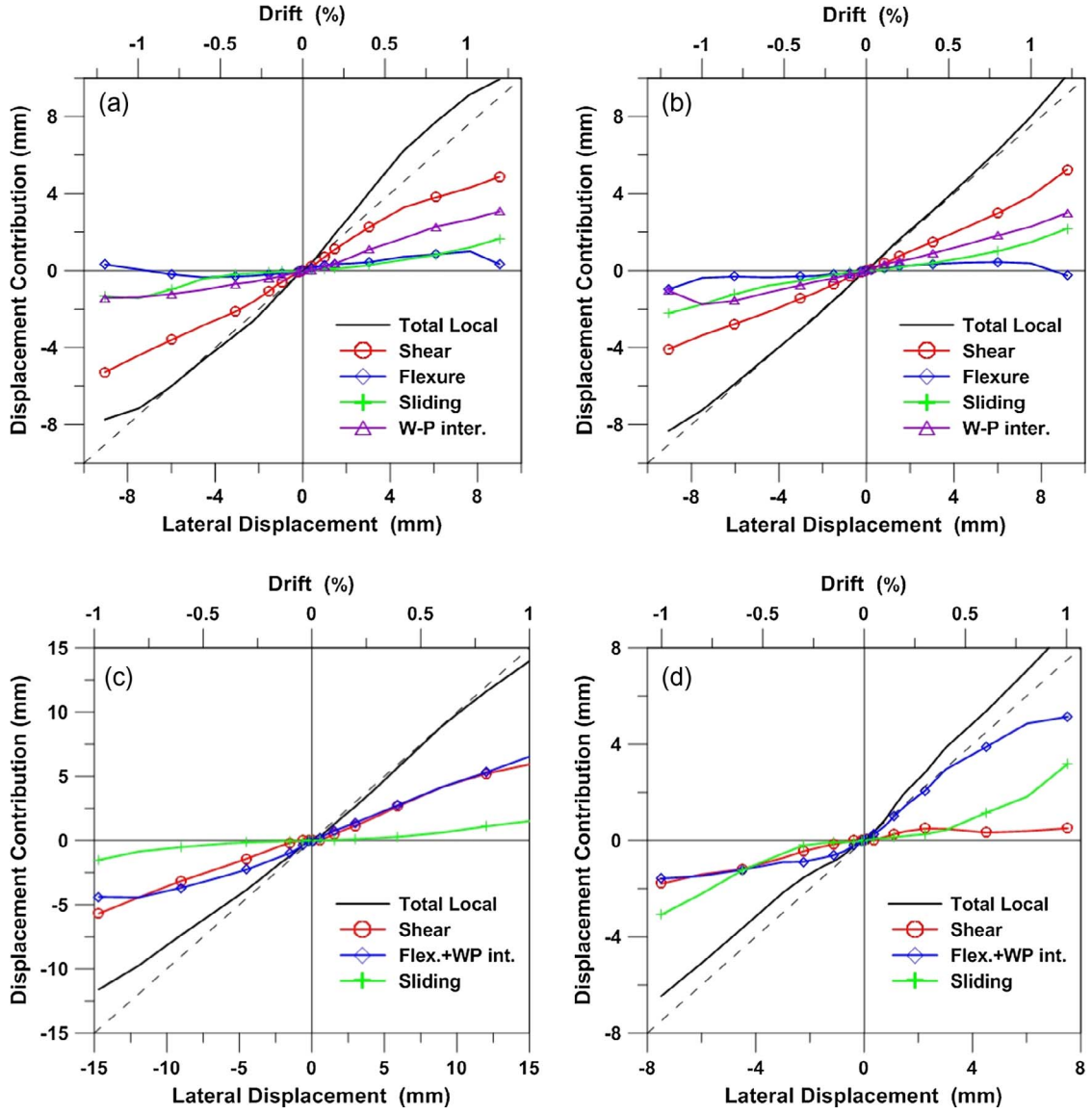

Fig. 9. Local deformation contributions: (a) T1-N5-S1, (b) T2-S2, (c) T6-S1, (d) T3-S1.

backbone curve recommended in the ASCE 41-13 Commentary, which shows better correlation with the test results. The alternative approach in ASCE41-13, with sudden degradation in post-peak lateral load behavior, is also shown in the plots with a dashed line, which generally underestimates the lateral load during degradation behavior. Results for all other specimens can be found elsewhere (Terzioglu [22]).

The experimentally-measured drift levels at cracking, yield, and ultimate are presented for all specimens in Table 2. The cracking drift, δ_{cr}, is the drift level at the time of initial cracking. The yield drift, δ_y, is calculated using an idealized bilinear load-displacement curve, which is generated by approximately equating the areas under the idealized and the actual load-displacement envelopes, as the drift level at the idealized yield capacity. The ultimate drift, δ_u, is defined as the drift ratio corresponding to the displacement at 80% of the peak lateral load capacity after load degradation has started. Results presented in the Table 2 indicate that the specimens cracked at approximately 0.05–0.1% drift, and reached ultimate drift levels of approximately 1.2–1.6%. Ductility ratios of the specimens varied from 1.5 to 4.0. The largest drift capacity was observed for Specimen T5-S1 (1.6%), which had an aspect ratio of 1.0 and low amount of longitudinal web reinforcement (0.34%).

2.6.1. Diagonal tension specimens

Fig. 7(a) compares the experimental lateral load vs. top displacement response (and its envelop) with the ASCE 41 backbone curve for specimen T1-S1, which experienced diagonal tension failure. The lateral load degrades soon after the lateral load capacity is reached, which is indicative of failure due to crushing of concrete. The hysteresis loops show high pinching for the loading cycles after the capacity is reached. The specimen shows a residual strength of approximately 15% of the capacity at the high drift levels. The ASCE 41 backbone relationship can reasonably represent the initial and post-cracking stiffness of the wall. The shear strength prediction of ACI 318 (i.e., the capacity of the ASCE 41 backbone curve) slightly underestimates the experimental lateral load capacity of the wall. The ASCE 41 backbone curve more accurately represents the lateral load degradation attributes of the response when the original backbone curve (shown in dashed line) is modified as suggested in ASCE 41 Commentary, by using a straight line segment from peak capacity at 1% drift to residual capacity at 2% drift (shown in solid line).

Specimen T1-S2, had identical geometry and reinforcement to T1-S1, but incorporated confinement at the boundaries. The overall load-displacement response (Fig. 7(b)) presents similar lateral load capacity, although a little bit lower, which is possibly associated reduction in the

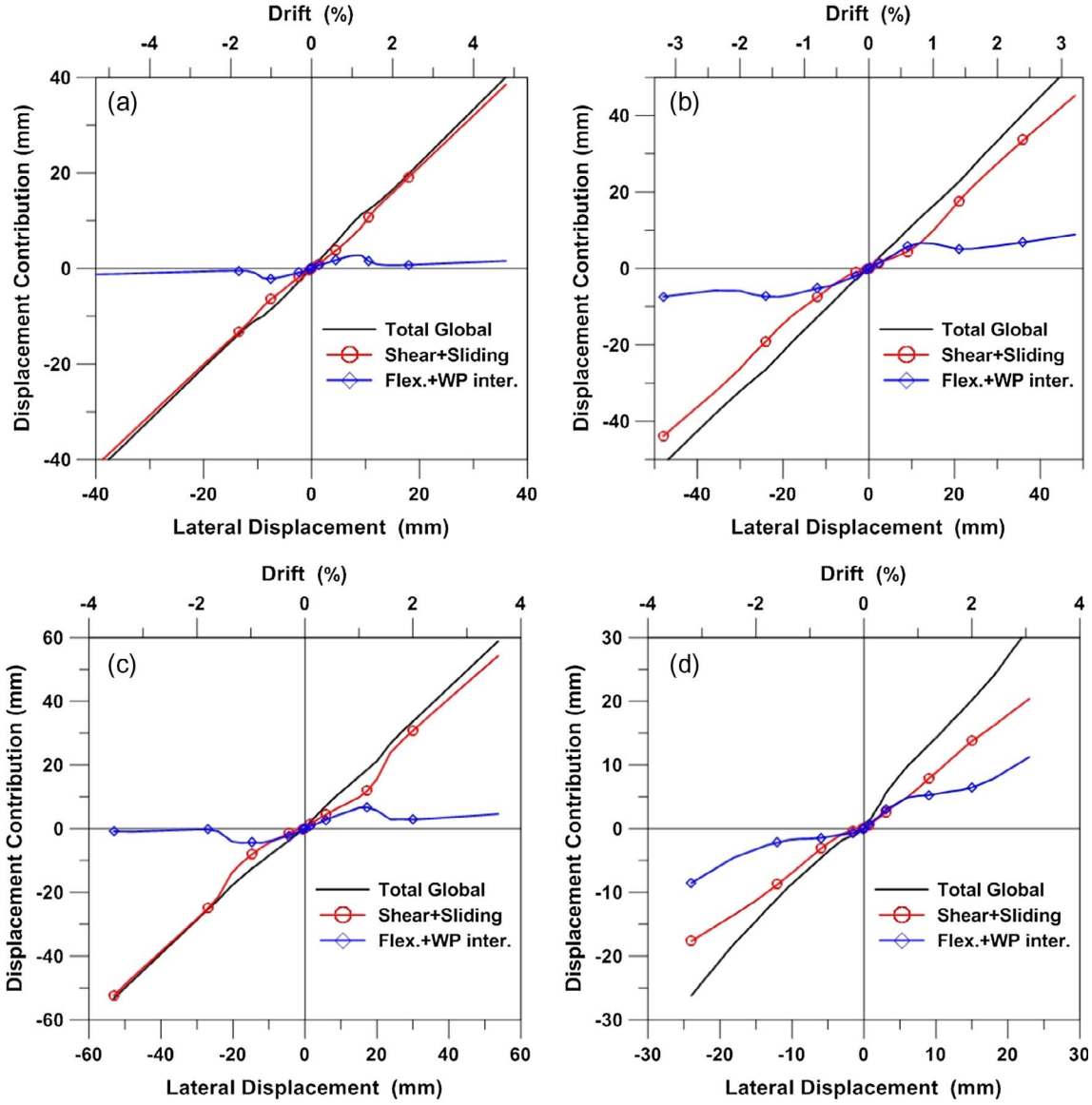

Fig. 10. Global deformation contributions: (a) T2-S2, (b) T5-S1, (c) T6-S1, (d) T3-S1.

Table 2
Comparison of lateral load capacity with ACI-318 predictions, experimental lateral deformation capacities, and observed failure modes.

Specimen	V_{cr} (kN)	V_u[1] (kN)	$V_{n,ACI}$[2] (kN)	$V_{n,ACI-SF}$[3] (kN)	$V_{n,ACI-FLEX}$[4] (kN)	V_u/V_n	δ_{cr} (%)	δ_y (%)	δ_u (%)	δ_u/δ_y	Failure Mode
T2-S1	254	799	656	695	835	1.22	0.1	0.8	1.2	1.5	Diag. Comp.
T2-S2	212	666	759	923	850	0.88	0.1	0.8	1.2	1.5	
T2-S3	380	813	805	1012	855	1.01	0.1	0.4	1.2	3.0	
T3-S1	255	383	846	709	480	0.80	0.1	0.3	1.2	4.0	Sliding
T4-S1	360	874	881	1095	1180	0.99	0.05	0.4	1.4	3.5	Diag. Comp.
T5-S1	170	710	618	1098	785	1.15	0.05	0.4	1.6	4.0	
T6-S1	140	735	710	813	870	1.04	0.05	0.6	1.4	2.3	
T1-S2	160	563	572	864	690	0.98	0.05	0.6	1.2	2.0	Diag. Tens.
T1-N5-S1	300	789	583	945	825	1.35	0.05	0.6	1.2	2.0	
T1-N10-S1	275	793	590	997	970	1.34	0.05	0.6	1.2	2.0	
T1-S1	180	635	525	853	690	1.21	0.05	0.8	1.2	1.5	

Note: 1 kN = 0.225 kips.
[1] Average of maximum lateral load measured in positive and negative directions.
[2] Nominal shear strength per ACI 318-14.
[3] Nominal shear friction capacity per ACI 318-14.
[4] Nominal flexural lateral load capacity per ACI 318-14.

effective area of concrete at the boundaries due to the confinement. However, the strength degradation behavior of this specimen is significantly different than that on T1-S1. A residual strength of approximately 45% of the lateral load capacity was reached at 2% drift level, and the specimen maintained its residual strength up to 4.8% drift. The lateral load on this specimen also degrades more gradually than T1-S1, allowing better hysteretic energy dissipation. The improved degradation characteristics and residual capacity of the specimen is attributed to the confined boundary regions. For this specimen, although the ASCE 41 backbone curve provides a slightly unconservative strength prediction in the positive loading direction, the estimated load-displacement behavior is good up to the residual strength drift level of 2%. However, while the specimen had a residual capacity of approximately 45% of peak capacity, the ASCE 41 backbone predicts only 20% residual strength.

Specimen T1-N10-S1 (Fig. 7(c)) was tested under an axial load level of $10\%A_g f_c'$. The specimen showed very sudden lateral load degradation after capacity was reached. The lateral load capacity of this specimen was higher by 25%, compared to an identical specimen (T1-S1) on which no axial load was applied. The specimen experienced a very sudden load decrease at approximately 1% drift. It lost almost all of its lateral load capacity during the subsequent two drift levels to 1.2% and 1.4%. No further drift levels were applied on the specimen. At 1.4% drift, the wall was maintaining its axial load carrying capacity. For this specimen, although the ASCE 41-13 lateral load capacity prediction (per ACI 318-14) is approximately 25% lower than the test result, the pre-crack and post-crack stiffness characteristics of the wall were reasonably represented. As well, the degradation in lateral load was captured reasonably well by the ASCE 41 backbone, which reduces the lateral load from the capacity at 0.75% drift to zero at 1% drift. For both of the axially-loaded specimens, the ACI-318 nominal shear strength estimate was approximately 25% lower than the experimentally-measured lateral load capacity.

2.6.2. Diagonal compression specimens

A total of six wall specimens experienced diagonal compression failure. For three of these specimens, the ACI 318-14 shear strength predictions are very close to experimentally-measured capacities, whereas the predictions are 15%–20% conservative for two of them. Only for specimen T2-S2, the ACI 318-14 shear strength estimate was approximately 10% lower than measured (Table 2).

All Type 2 specimens were tested under zero axial load, and had high vertical and horizontal web reinforcement ratios of (0.68%). Fig. 7(d) compares the experimental load–displacement response obtained for Specimen T2-S3 with the ASCE 41-13 backbone curve. The first main diagonal crack on this specimen formed at 0.15% drift, at 56% of the lateral load capacity. The capacity was reached at 0.6% drift. The ASCE 41-13 backbone curve model closely captures the overall response characteristics of this specimen, including its lateral load capacity, stiffness reduction after cracking, and ductility A much better representation of the strength degradation characteristics of the experimental envelop curve is achieved by using a linear variation in lateral load from the lateral load capacity at 1% drift to zero load at 2% drift, as suggested in ASCE 41-13 Commentary 10.3.1.2.2.

Specimen T2-S1 had horizontal U-cap hooks at the wall boundaries, which differentiated it from all specimens that incorporated 180° hooks at the ends of horizontal web reinforcement. The overall load-displacement response of T2-S1 was similar to other Type 2 specimens, indicating that having U-caps or 180° hooks for anchorage of the horizontal web reinforcement, did not significantly influence the response. Type 2 specimens, as well as specimens of Type 4, 5 and 6, failed in diagonal compression. The overall load–displacement response characteristics of all of these specimens were similar, and they also do not differ substantially from other specimens that failed in diagonal tension, except for specimen T5-S1, which experienced less strength degradation and larger residual capacity (Fig. 7(e)).

Specimen T5-S1 showed the most ductile lateral load behavior among all specimens tested. It also demonstrated higher ductility compared to the other one-aspect-ratio specimen (T6-S1). This is due to the low amount of vertical web reinforcement in Specimen T5-S1, which experienced yielding of boundary reinforcement and most of the vertical web reinforcement at the onset of lateral load capacity. Yielding of vertical bars resulted in significant contribution of flexural deformation to wall lateral displacement, and increased the displacement ductility of the specimen and its residual strength. The ASCE 41-13 backbone curve represents the initial stiffness of this wall reasonably well, but notably underestimates its cracked stiffness, lateral load capacity, and residual strength.

2.6.3. Sliding shear specimen

The observed failure mode of Specimen T3-S1 showed that when a squat wall has low amount of boundary reinforcement, so that flexural yielding occurs before the shear-friction capacity is reached, and if the shear-friction capacity of the wall is also lower than its nominal shear strength, the wall may fail in a premature sliding shear mode triggered by cracking and reinforcement yielding at the wall-pedestal interface, before even the nominal flexural capacity is reached. The interface crack on this specimen first formed at 0.1% drift, at 65% of its lateral load capacity, after which the wall did not experience any significant diagonal cracking or shear deformation. The specimen reached its lateral load capacity at approximately 0.3% drift.

Fig. 7(f) compares the experimental load-displacement response with the ASCE 41-13 backbone curve generated for this specimen for Specimen T3-S1. The lateral load capacity of this wall was significantly lower than all others. The measured load-displacement response of this specimen was somewhat unsymmetrical in positive and negative loading directions, with peak capacities of 440 kN and 320 kN in the positive and negative directions, respectively. This was due to asymmetry in the flexural yielding behavior (flexural deformation contributions to lateral displacement), as described in the previous section. The degradation in lateral load after reaching capacity was much more gradual in this wall compared to most of the other specimens. The flexural lateral load capacity estimated for this wall per ACI-138 Section 22.2 is smaller than both its shear-friction capacity its nominal shear strength. Therefore, the ASCE 41-13 backbone curve was generated considering that this is a flexure-controlled wall, as illustrated in Fig. 6(a). In terms of the overall load-displacement response, the ASCE 41-13 backbone curve overestimates the stiffness, lateral load capacity, ductility, and residual strength of this wall, although the rate of degradation in lateral load is coincidentally well-captured.

3. Summary and conclusions

The objective of this experimental study was to investigate the lateral load behavior of squat reinforced concrete walls, for better understanding and representation of their behavioral characteristics including lateral load capacity, ductility, strength degradation attributes, and potential failure modes. The wall specimens investigated were differentiated by their aspect ratios, amounts of horizontal and vertical web reinforcement, amounts of boundary reinforcement, and axial load levels. The results and conclusions of this study are summarized below:

- The behavior and failure modes of all the test specimens investigated were shear-controlled. The three types of failure observed for the test specimens were diagonal tension failure (associated with concrete crushing along diagonal struts), diagonal compression failure (crushing initiating at bottom corners propagating along the wall base), and sliding shear failure at wall base, triggered by cracking at the wall-pedestal interface and flexural yielding of boundary reinforcement.
- It was observed that the horizontal and vertical web reinforcement ratios of the walls are critical in determining whether a diagonal

tension failure or a diagonal compression failure will develop. In these tests, regardless of the wall aspect ratio and axial load level, specimens with 0.34% web reinforcement ratio experienced diagonal tension failure, whereas specimens with 0.68% web reinforcement ratio experienced diagonal compression failure. Specimens with axial load, although subjected to large average shear stress demands at capacity, also failed in diagonal tension, due to low amount of web reinforcement.

- Comparing the test results for the specimens with aspect ratio of 1.0, the amount of vertical web reinforcement was found to influence both the lateral load capacity and the distribution of the diagonal cracks. Increased vertical web reinforcement ratio resulted in increase in the lateral load capacity, and also provided a more uniformly-distributed crack pattern, with more frequent cracks.
- It was observed that using a low amount of longitudinal boundary reinforcement can cause a premature sliding shear type of failure at the interface of the wall, triggered by flexural cracking and yielding of boundary longitudinal reinforcement, before either the nominal flexural capacity or the shear-friction capacity is reached.
- The lateral load capacities calculated according to ACI 318-14 were reasonably close to the experimentally-measured capacities of most of the wall specimens, and were slightly conservative (by 15–20%) for others. For the axially-loaded specimens, the ACI 318-14 equation underestimated the shear strength of the specimens by approximately 25%
- The lateral load vs. displacement response of all specimens were dominated by shear deformations. Lateral load degradation was rapid after the capacity was reached. In general, the specimens showed poor ductility characteristics, as expected for squat walls. The specimen with confined boundary zones showed significantly higher residual strength, and favorable ductility characteristics at the residual strength level.
- It was confirmed that axial load on a squat wall increases its lateral load capacity, but has negative effect on ductility characteristics and the residual capacity. Axially-loaded wall specimens showed significantly lower residual load capacities and poor ductility characteristics, compared with the zero-axial-load specimens that failed in diagonal tension. It was observed that higher levels of axial load on a wall (e.g., 10% of axial load capacity) can result in very rapid degradation of its lateral load capacity.
- It was observed that the ASCE 41-13 backbone curves defined for shear-controlled walls, were reasonable in predicting the lateral load vs. displacement response characteristics of the wall specimens tested, despite underestimating the residual strength of the specimen with confined boundaries and the specimen that experienced flexural yielding simultaneously with shear failure. The approach suggested in the ASCE 41-13 Commentary for consideration of linear degradation in lateral load on the backbone curve represented the experimentally-observed degradation behavior much more closely.

Acknowledgements

Financial support for this project provided by Chile's National Commission on Scientific and Technological Research (CONICYT) for the project Fondecyt 2008, Initiation into Research Funding Competition, under Grant No. 11080010, is gratefully acknowledged.

References

[1] Paulay T, Priestley MJN. Seismic design of reinforced concrete and masonry buildings. New York: John Wiley & Sons Inc.; 1992. p. 362–3.
[2] Massone LM, Orakcal K, Wallace JW. Modeling of squat structural walls controlled by shear. ACI Struct J 2009;106:646–55.
[3] Cardenas AE, Hanson JM, Corley WG, Hognestad E. Design provisions for shear walls. ACI J 1973;70:221–30.
[4] Barda F, Hanson JM, Corley WG. Shear strength of low-rise walls with boundary elements. ACI Special Publ 1977;53:149–202.
[5] Wood SL. Shear strength of low-rise reinforced concrete walls. ACI Struct J 1990;87:99–107.
[6] Collins MP, Mitchell D. Rational approach to shear design-the 1984 Canadian code provisions. J Proc 1986;83:925–33.
[7] Benjamin JR, Williams HA. Blast and earthquake resistant design data: behavior of one-story reinforced concrete shear walls containing openings. J Proc 1958;55:605–18.
[8] Cardenas A, Russell H, Corley W. Strength of low-rise structural walls. ACI Special Publ 1980;63:221–42.
[9] Hidalgo PA, Ledezma CA, Jordan RM. Seismic behavior of squat reinforced concrete shear walls. Earthq Spectra 2002;18:287–308.
[10] Lefas ID, Kotsovos MD, Ambraseys NN. Behavior of reinforced concrete structural walls: strength, deformation characteristics, and failure mechanism. ACI Struct J 1990;87:23–31.
[11] Salonikios TN, Kappos AJ, Tegos IA, Penelis GG. Cyclic load behavior of low-slenderness reinforced concrete walls: design basis and test results. ACI Struct J 1999;96:649–60.
[12] FEMA 356. Prestandard and commentary for the seismic rehabilitation of buildings. Washington, DC: Federal Emergency Management Agency; 2000.
[13] Orakcal K, Massone LM, Wallace JW. Shear strength of lightly reinforced wall piers and spandrels. ACI Struct J 2009;106:455–65.
[14] Massone LM. RC wall shear – flexure interaction: analytical and experimental responses [PhD. thesis]. Los Angeles: University of California; 2006.
[15] ASCE 41-13. Seismic rehabilitation of existing buildings. Reston (Virginia): American Society of Civil Engineers; 2013.
[16] ACI 318-14. Building code requirements for structural concrete and commentary. Farmington Hills (MI): American Concrete Institute; 2014.
[17] Hsu TT, Mo Y. Softening of concrete in low-rise shearwalls. ACI J Proc 1985.
[18] Hwang S-J, Fang W-H, Lee H-J, Yu H-W. Analytical model for predicting shear strengthof squat walls. J Struct Eng 2001;127:43–50.
[19] Kolozvari K, Tran TA, Orakcal K, Wallace JW. Modeling of cyclic shear-flexure interaction in reinforced concrete structural walls. II: Experimental validation. J Struct Eng 2014;141.
[20] Rojas F, Anderson JC, Massone LM. A nonlinear quadrilateral layered membrane element with drilling degrees of freedom for the modeling of reinforced concrete walls. Eng Struct 2016;124:521–38.
[21] Gullu MF, Orakcal K. Nonlinear finite element modeling of reinforced concrete structural walls. In: 16th World conference on earthquake engineering, Santiago, Chile; 2017.
[22] Terzioglu T. Experimental evaluation of the lateral load behavior of squat structural walls. Istanbul (Turkey): Boğaziçi University; 2011.
[23] Park R, Paulay T. Reinforced concrete structures. New York: Wiley; 1975. p. 618–22.
[24] Massone LM, Wallace JW. Load-deformation responses of slender reinforced concrete walls. ACI Struct J 2004;101:103–13.